scientific reports

Check for updates

OPEN

The depth of tumor hierarchy and its impact on hypertumor susceptibility

Jibeom Choi[1,2]✉, Suhyeon Kim[1], Sunmi Lee[1] & Junpyo Park[1]✉

Cancer cells, despite their shared origin, could be heterogeneous with respect to their stemness, plasticity, self-renewal, and oncogenicity. Recent findings indicate that a small proportion of the cancer cells oligopolize the capacity to produce diverse cancer subtypes and metastasize to other sites. Analogous to the apical hierarchy observed in adult stem cells, such versatile cancer cells were termed cancer stem cells. Meanwhile, hypertumors that exploit the cooperation of other cancer cells may disrupt the integrity of the tumor, prompting tumor regression. The biology of cancer stem cells and hypertumors has substantial clinical potential, but no study up to date has investigated the effect of cancer hierarchy on hypertumor progression. In this study, we developed biologically relevant models that elucidate the dynamics of hypertumor progression under different hierarchical structures. Our models align with previously observed data from human breast cancer subpopulations capable of state transitions. We tested and compared the progression dynamics of cancer clusters with different characteristics. Considering the trade-off between proliferation and mutation risk, our computational results suggest that existence of the cancer stem cells with high self-renewal and replication could be the prerequisite for attaining larger cancer size. In contrast, if a small cancer size is sufficient to induce lethality, a tumor composed of homogeneous cells would take less time to reach such a threshold size. Consequently, the hierarchical structure of cancer that reaches a lethal size may vary across species, representing a relevant mechanism of Peto's paradox. The formulations presented in this study link the less attended aspects of cancer which would provide integrative insights for therapeutic strategies.

Mankind still being afflicted by cancer, facets of cancer that have gained minor clinical attention could be the cornerstone for developing transformative therapeutic applications. One such facet is the existence of the cancer hierarchy. Lines of empirical evidence suggest that not all cells in a tumor have the capacity to form another cluster of tumors (tumorigenicity). Comparable to the stem cells of normal tissue, a small subpopulation in a tumor endowed with tumorigenicity and self-renewal can generate diverse types of cancer cells, referred to as cancer stem cells (CSCs)[1–4]. At least in some cancers, CSCs produce identical CSCs or other cancer cells that lack tumorigenicity called bulk tumor cells or non-CSCs[1]. The distinction between CSCs and bulk tumor cells established the conceptualization of hierarchical organization in cancer (cancer stem cell model), rather than an aggregation of homogeneous mutated cells.

The CSC has significant clinical implications as a small number of the CSCs that are not eliminated by therapy would elicit relapse with a poorer prognosis (minimal residual disease)[5]. Moreover, it is commonly accepted that CSCs are more resilient to conventional therapies, presumably due to their dormancy[3]. Though selective elimination of CSCs will confer improved prognosis, off-target effects of such therapy may have detrimental effects on normal stem cells as both types of cells have multiple traits in common[2].

However, there is a wide range of disputes concerning the technical pitfalls of experiments designed to verify the existence and characteristics of CSCs[2,3]. The ordinary procedure to elucidate CSCs is the xenograft assay whereby cancer cells of the same type are engrafted to immunosuppressed animals. Although a specific type of cancer cells sorted by surface markers can form a tumor or induce leukemia in immunosuppressed animals, this does not fully validate the hierarchy of cancer. Incompatibility of cancer growth factors across species, heterotopic transplant, lack of appropriate tumor microenvironment, and the effect of the cell sorting obscure the interpretation of the results obtained from xenograft assay[2,6,7]. In addition, the cell surface markers used to classify the cancer cell types might be uninformative[3].

On the other hand, some types of cancers do not exhibit a hierarchical structure. Most cancer cells of melanoma and a specific type of leukemia have tumorigenicity (or leukemia-initiating capability), which

[1]Department of Applied Mathematics, College of Applied Sciences, Kyung Hee University, Yongin 17104, Republic of Korea. [2]School of Computational Sciences, Korea Institute for Advanced Study, Seoul 02455, Republic of Korea. ✉email: snu10@snu.ac.kr; junpyopark@khu.ac.kr

confirms the absence of hierarchy[2,8,9]. The lack of hierarchy might be attributed to the frequent interconversion of tumorigenic (or leukemia-initiating) state and non-tumorigenic state[1]. The high explanatory power of the stochastic Markov model on the subtype frequency of breast cancers implies that state transitions underlie the phenotypic equilibrium within the cancer cluster[10]. Though hardwired stemness has been a canonical framework in theories of stem cells and CSCs, observations obtained from lineage-tracing methods provide stronger support for the higher prevalence of plasticity in the hierarchy than previously estimated[1]. Hierarchy also could be less distinctive if a tumor is saturated with cancer cells that gained stemness by accumulated mutations[3].

The evolutionary dynamics of cancer without explicit hierarchy are explained by the clonal selection model of cancer progression[2,3]. Analogous to theories of natural selection[11], replication of cancer cells will result in the formation of subclones composed of slightly different genotypes, and those subclones that are equipped with higher fitness will be selected for and proliferate[2,3]. The pattern of branching evolution found in certain cancers is coherent to this model[12–15].

It merits particular attention that CSC theory and clonal selection theory are not mutually exclusive[2–4]. Neither model alone can explain the general progression dynamics of cancers [2,3]. For example, the clonal selection model alone cannot interpret cancer composed of a hardwired hierarchy in which a few cells produce bulk tumor cells without the interconversion of states. On the other hand, the CSC model is inapplicable to cancer composed of equipotent cells without hierarchy. Rather than adopting a single framework, both models can collectively explain the cancer progression. Within each subpopulation, there could be variability in each cell, and some of the cells may work as CSCs for that subpopulation[3,16]. As CSCs exhibit genetic diversity[14,17], the clonal selection model can be employed to describe the competitive dynamics of hierarchical subpopulations, where the presence of such hierarchy requires the application of the CSC model[2,3]. A mathematical model that postulated hierarchical structure and state transition reliably illustrated empirical results, demonstrating the coordination of the CSC model and clonal selection model[18]. The nature of the CSCs and corresponding cancer hierarchy holds substantial clinical implications which will pave the way for reliable and effective cancer therapies[2,3].

Another underexplored facet of cancer is the social cooperation[19]. Cancer cells emit diverse growth factors such as IGF-2 or TGF-β that promote the fitness of the conspecific cancer cells in an autocrine and paracrine manner[19–21]. As it is metabolically costly to produce those growth factors, production of them is a form of cooperation among cancer cells[19]. Some cancer cells may take advantage of growth factors produced by other cancer cells while not producing them[22,23]. Such cheaters were referred to as hypertumors, coined to imply the 'tumor of tumor[22,23]'. Compared to the CSC model, this paradigm is in its infancy: While a plethora of empirical experiments were performed to verify the CSC model, few, if any, experiment was conducted to investigate the hypertumor[24]. Nonetheless, implementation of the artificially manufactured hypertumor into the tumor cluster may lead to tumor regression by interfering the intratumor cooperation, a concept labeled as autologous cell defection[24,25]. Mathematical models, spatial simulations, and a set of in vitro experiments revealed the clinical potential of this approach[21,25,26]. Meanwhile, the emergence of hypertumor is speculated to be one of the underlying factors of Peto's paradox[23,27]. Peto's paradox refers to the absence of a significant correlation between cancer susceptibility and cell number (or life span) across species[27]. This lack of correlation is intriguing because it is natural to expect that a larger number of cells and a longer lifespan during which mutations accumulate facilitate carcinogenesis[28]. In the same line with this speculation, body mass and age elevate the cancer risk when analyzed within a species. For example, intraspecific comparisons of domestic dogs and humans support a positive correlation between body size and cancer risk[29]. Other factors including size-dependent metabolic rates, evolutionary pressure for costly tumor-suppression mechanisms, or elaborate immune systems were proposed as underlying mechanisms of Peto's paradox[29–32].

Cancer hierarchy and intratumor cooperation mechanism are the decisive features of cancer that could reconstruct our understanding of cancer to develop translational clinical approaches. Although numerous studies focused on the dynamics of CSC progression were proposed[33–35], to our knowledge, there has been no in-depth study that analyzed the effect of cancer hierarchy on the development of hypertumor. In this study, we developed mathematical models that reflected diverse possible hierarchies of cancer to estimate their impacts on hypertumor. Our formulations imply that the hierarchy of cancer that reaches the lethal size could be different across species[36].

Evolutionary dynamics of cancer cells without hierarchy

Evolutionary dynamics when state transition is not allowed

As in the case of melanoma, most cancer cells (other than those that are damaged or senescent) may possess the homogeneous replication capability[2,8,9]. Under this scheme, the state transition was not postulated and all cancer cells were assumed to be equipotent. It should be noted that intratumor heterogeneity does not guarantee the existence of hierarchy because branching evolution with multiple subpopulations suffices to explain such heterogeneity[2]. Therefore, to refer to the condition that all cancer has similar cancer-initiating capability without ambiguity, the term homogeneous cancer model (henceforth, HC model) will be used in this study.

For each replication, there is a possibility that hypertumor may arise by mutation at growth-factor-producing genes[21,24,25], as malfunction of such genes can transform the cancer cell into the hypertumor[24]. Mutations in other genes involved in establishing the tumor microenvironment, such as *Vegfa* for angiogenesis, can also lead to hypertumor formation[22].

For a cancer cluster of cell number $N_C(t)$ at time t (excluding hypertumors), suppose that cancer cells have a replication rate of R_0 and decay rate of δ_0. μ represents the degree of mutation that contributes to the emergence of hypertumors during cancer cell replication (Fig. 1a,b). Then, the following differential equation can be derived.

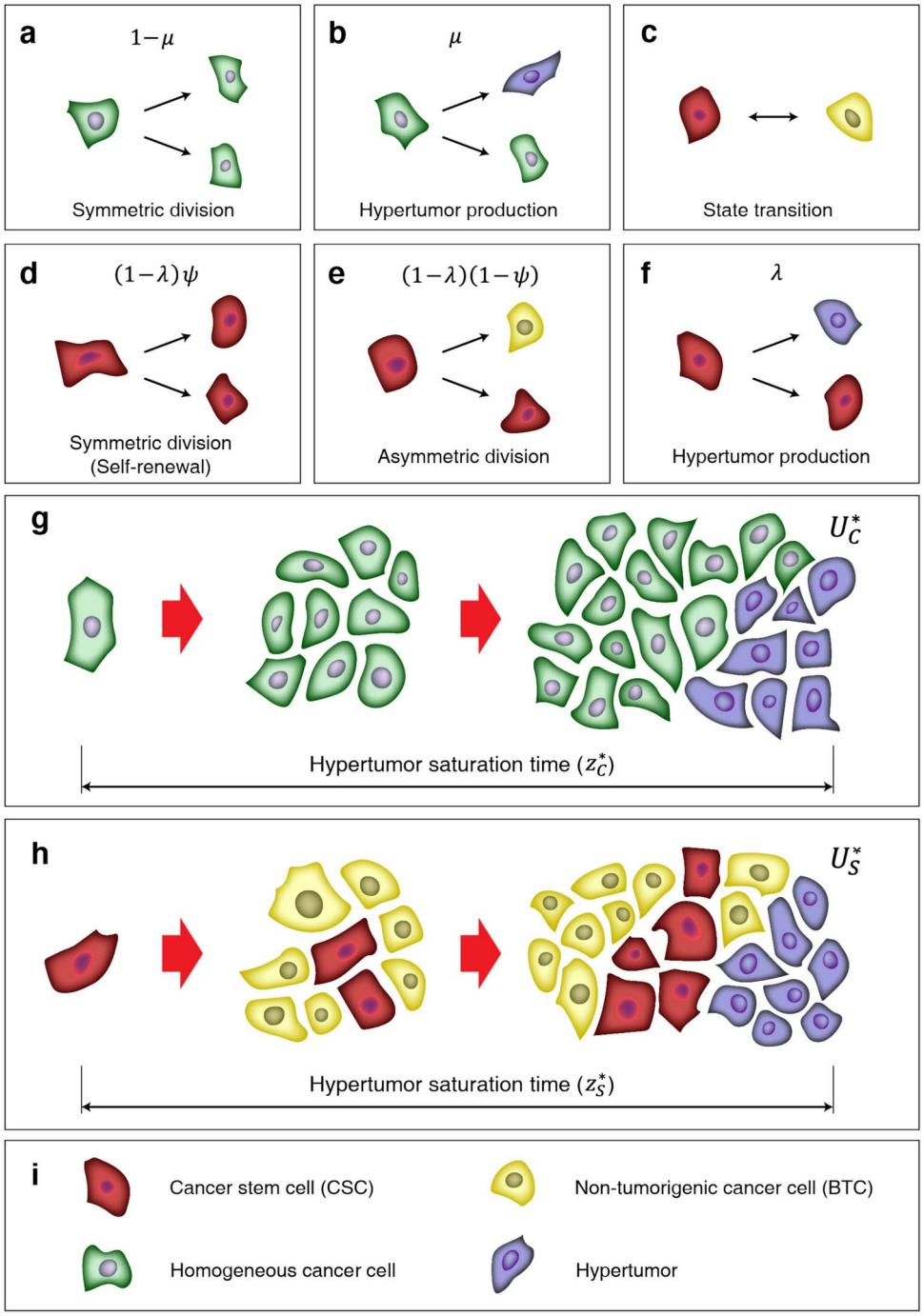

Fig. 1. The illustration of the cancer progression under the homogeneous cancer model (HC model) and cancer stem cell model (CSC model). (**a**) Under the HC model, cancer cells (green cells) produce identical progeny cells given that mutation does not occur with the probability of $1-\mu$. (**b**) During the replication, hypertumors (blue cells) may appear as a result of mutation with the probability of μ. (**c**) If the rate of state transition among cells is sufficiently higher compared to that of the replication, the cluster of cancer will act similarly to the homogeneous cluster. (**d**) Under the CSC model, cancer stem cells (red cells) may generate an identical CSC with the probability of $(1-\lambda)\psi$. Here, $(1-\lambda)$ represents the probability that mutation does not occur. (**e**) Likewise, with the probability of $(1-\lambda)(1-\psi)$, a CSC produces a bulk tumor cell lacking stemness. (**f**) Due to a mutation, a hypertumor may arise during the replication of a CSC. (**g**) Under the HC model, if the ratio of hypertumors reaches a certain threshold, the cancer growth is arrested. Hypertumor saturation time refers to the duration it requires for hypertumors to reach such a ratio. The cancer size at hypertumor saturation time is defined as the eventual cancer size (U_C^*). (**h**) Same as (**g**) for the CSC model. (**i**) The graphical illustration of the cells described in (**a**)–(**h**).

$$\frac{dN_C(t)}{dt} = ((1-\mu)R_0 - \delta_0)N_C(t). \tag{1}$$

For simplicity, take $\omega_0 = (1-\mu)R_0 - \delta_0$ which refers to the net growth rate of the cancer cells. The sign of ω_0 determines whether the cancer size increases or decreases as time goes by, which is occasionally termed the realized intrinsic rate of increase or the Malthusian parameter[37].

Given that the number of cancer cells at the beginning is 1 ($N_C(0) = 1$),

$$N_C(t) = \exp[((1-\mu)R_0 - \delta_0)t] = \exp[\omega_0 t] \tag{2}$$

where $\exp[x] = e^x$.

While tumor growth may follow the exponential regime at the early stage, the growth at the later stage could be impeded due to the inaccessibility to nutrients or oxygen[38]. The impeded tumor growth under in vivo conditions is considered in computational simulation by replacing the time terms of the general solutions (see Computational analysis).

Let $H_C(t)$ denote the number of hypertumor cells at time t under the HC model. The replication rate of the hypertumor is $R_{H,C}$ sharing the same decay rate with the normal cancer cells.

$$\frac{dH_C(t)}{dt} = (R_{H,C} - \delta_0)H_C(t) + \mu R_0 N_C(t) \tag{3}$$

where $\mu R_0 N_C(t)$ corresponds to the mutation of the newly replicated cancer cells that supply the hypertumor population. Similar to ω_0, take $\omega_{H,C} = R_{H,C} - \delta_0$ which represents the net growth rate of hypertumor. Given that $H_C(0) = 0$, the solution of Eq. (3) is

$$H_C(t) = \frac{\mu R_0}{\omega_{H,C} - \omega_0}(\exp[\omega_{H,C}t] - \exp[\omega_0 t]). \tag{4}$$

Suppose N^* is the minimal number of cancer cells that leads to lethality. Put another way, if the number of cancer cells reaches N^*, the organism dies. Take t_C^* as the time it takes for the cancer cell number to reach N^* after the first appearance of the cancer cell. Based on Eq. (2),

$$t_C^* = \frac{\ln[N^*]}{\omega_0}. \tag{5}$$

where $\ln[x]$ is the natural logarithm of x.

Similarly, suppose that there is a critical ratio ρ_H^* such that the cancer cluster cannot grow anymore if the ratio of the hypertumor cells to the cancer cluster is above ρ_H^*. Take z_C^* as the time it takes for the hypertumor ratio becomes ρ_H^* after the first appearance of the cancer cell. As $H_C(z_C^*)/N_C(z_C^*) = \rho_H^*$ should hold,

$$z_C^* = \frac{1}{\omega_{H,C} - \omega_0}\ln\left[1 + \left(\frac{\omega_{H,C} - \omega_0}{\mu R_0}\right)\rho_H^*\right]. \tag{6}$$

Let the hypertumor saturation time (HST) denote the time it takes to reach the critical hypertumor ratio (Fig. 1g). Let the eventual cancer size (U_C^*) denote the cancer size at HST (z_C^*).

Evolutionary dynamics when state transition is allowed

On the other hand, state transition between subpopulations can be postulated (Fig. 1c). Let $V_i(t)$ denote the number of cells of the i-th subpopulation at time t. With a certain probability, some cells in the i-th subpopulation may transform into the j-th subpopulation ($i \neq j$). Such state transition can be formulated as follows.

$$\frac{dV_i(t)}{dt} = \eta_i V_i(t) + \sum_{j\neq i}\tau_{j,i}V_j(t), \tag{7}$$

$$\eta_i = R_i - \delta_i - \sum_{j\neq i}\tau_{i,j} \tag{8}$$

where $\tau_{j,i}$ is the rate of state transition from the j-th to the i-th subpopulation. R_i and δ_i are the replication rate and the decay rate of the i-th subpopulation, respectively.

Given that there are m subpopulations, we can formulate the following matrix differential equation.

$$\dot{\mathbf{V}}(t) = \begin{bmatrix} V_1'(t) \\ V_2'(t) \\ V_3'(t) \\ \vdots \\ V_m'(t) \end{bmatrix} = \begin{bmatrix} \eta_1 & \tau_{2,1} & \tau_{3,1} & \cdots & \tau_{m,1} \\ \tau_{1,2} & \eta_2 & \tau_{3,2} & \cdots & \tau_{m,2} \\ \tau_{1,3} & \tau_{2,3} & \eta_3 & \cdots & \tau_{m,3} \\ \vdots & \vdots & \vdots & \ddots & \vdots \\ \tau_{1,m} & \tau_{2,m} & \tau_{3,m} & \cdots & \eta_m \end{bmatrix} \begin{bmatrix} V_1(t) \\ V_2(t) \\ V_3(t) \\ \vdots \\ V_m(t) \end{bmatrix} = \mathbf{Q}\mathbf{V}(t). \tag{9}$$

For brevity, assume that $\mathbf{Q}$ has distinct real eigenvalues. Then, the general solution is

$$V_i(t) = \sum_{j=1}^{m} b_{i,j}\exp[\lambda_j t] \tag{10}$$

where λ_i is the i-th eigenvalue of $\mathbf{Q}$ and $b_{i,j}$'s are coefficients determined by the initial condition and the eigenvectors.

Without loss of generality, take λ_1 as the largest eigenvalue (principal eigenvalue). For an i-th subpopulation whose coefficient of $\exp[\lambda_1 t]$ is not zero ($b_{i,1} \neq 0$), the following holds.

$$\lim_{t\to\infty} \frac{V_i(t)}{\sum_{j=1}^{m} V_j(t)} = \frac{b_{i,1}}{\sum_{j=1}^{m} b_{j,1}}. \tag{11}$$

Consequently, state transition establishes stable heterogeneity of cancer clusters under specific conditions even in the absence of the hierarchy.

In this study, it was defined that a subpopulation is persistent if its proportion in the total population does not tend to 0 as time tends to infinity. (Refer to Definition 2 of Supplementary Materials.) Hence, an i-th subpopulation with $b_{i,1} > 0$ is persistent. If a transition from an i-th persistent subpopulation to a j-th subpopulation is allowed ($\tau_{i,j} > 0$), then the j-th subpopulation is also persistent (Proposition 1 and corollaries). Detailed mathematical analyses are presented in Supplementary Materials.

Evolutionary dynamics under the hierarchy of cancer stem cell

Evolutionary dynamics when state transition is not allowed

As underpinned by a plethora of evidence, a cancer could be composed of CSCs that produce identical CSCs and bulk tumor cells (henceforth, BTCs). As a simpler model, it was assumed that the fate of each cell is hardwired. In other words, state transition was not postulated. Suppose that with the probability of ψ, a CSC produces a CSC during replication, and with the probability of $1-\psi$, a CSC produces a BTC, given that the mutation did not occur during the replication (Fig. 1d,e). The stochasticity of CSC to produce CSC or BTC is based on the empirical observation of CSC replication dynamics in skin papilloma through clonal analysis[39]. In our model, CSCs have a replication rate of R_S and decay rate of δ_S. Likewise, define R_P and δ_P as those of BTCs, matching R_S and δ_S, respectively. While normal adult stem cells can self-renew, normal differentiated somatic cells cannot persistently replicate (Hayflick limit)[40–42]. In parallel with such a relationship, BTCs have limited proliferative potential[40]. Hence, it is natural to postulate that $R_S - \delta_S \geq 0 > R_P - \delta_P$, implying that a cancer cluster solely composed of BTCs will eventually regress.

Hypertumors under the CSC model have a replication rate of $R_{H,S}$, whose decay rate is the same as that of the equipotent cancer cells under the HC model (δ_0). The degree of mutation that hypertumor is produced by CSC replication is λ (Fig. 1f). For simplicity, take $\overline{\psi} = 1-\psi$ and $\overline{\lambda} = 1-\lambda$.

Define ω_S as $\psi\overline{\lambda}R_S - \delta_S$, the net growth rate of CSCs. The net growth rate of BTCs is $\omega_P = R_P - \delta_P < 0$. It was assumed that replication of the BTCs does not produce hypertumor due to the lack of stemness in BTCs. Similarly, the net growth rate of hypertumor under the CSC model is $\omega_{H,S} = R_{H,S} - \delta_0$. The numbers of CSCs, BTCs, and hypertumor at time t under the CSC model are $N_S(t)$, $N_P(t)$, and $H_S(t)$, respectively. Given that $H_S(0) = 0$, $N_P(0) = 0$, and $N_S(0) = 1$, the following holds.

$$\frac{dN_S(t)}{dt} = \left(\psi\overline{\lambda}R_S - \delta_S\right) N_S(t), \tag{12}$$

$$\frac{dN_P(t)}{dt} = \overline{\psi}\,\overline{\lambda}R_S N_S(t) + \omega_P N_P(t), \tag{13}$$

$$\frac{dH_S(t)}{dt} = \left(R_{H,S} - \delta_0\right) H_S(t) + \lambda R_S N_S(t). \tag{14}$$

The general solutions are

$$N_S(t) = \exp\left[\left(\psi\overline{\lambda}R_S - \delta_S\right) t\right] = \exp\left[\omega_S t\right], \tag{15}$$

$$N_P(t) = \frac{\overline{\psi}\,\overline{\lambda}R_S}{\omega_S - \omega_P}\left(\exp\left[\omega_S t\right] - \exp\left[\omega_P t\right]\right), \tag{16}$$

$$H_S(t) = \frac{\lambda R_S}{\omega_{H,S} - \omega_S}\left(\exp\left[\omega_{H,S} t\right] - \exp\left[\omega_S t\right]\right). \tag{17}$$

Total cancer cell number is the summation of CSCs and BTCs, which can be approximated as

$$N_S(t) + N_P(t) \approx \left(\frac{\overline{\psi}\,\overline{\lambda}R_S}{\omega_S - \omega_P} + 1\right) \exp\left[\omega_S t\right] \tag{18}$$

because $\exp[\omega_P t]$ tends to 0 as t increases.

Let t_S^* denote the time it takes to reach the detrimental number of cancer cells under the CSC model. As $N_S(t_S^*) + N_P(t_S^*) = N^*$ should hold,

$$t_S^* = \frac{1}{\omega_S}\left(\ln\left[N^*\right] - \ln\left[1 + \frac{\overline{\psi}\,\overline{\lambda}R_S}{\omega_S - \omega_P}\right]\right). \tag{19}$$

HST under the CSC model (z_S^*) can be accordingly calculated.

$$z_S^* = \frac{1}{\omega_{H,S} - \omega_S} \ln\left[1 + \left(\frac{\overline{\psi}\,\overline{\lambda}R_S}{\omega_S - \omega_P} + 1\right)\left(\frac{\omega_{H,S} - \omega_S}{\lambda R_S}\right)\rho_H^*\right]. \tag{20}$$

Likewise, U_S^* is the eventual cancer size under the CSC model. Major variables are explained in Table 1.

Variable	Description
$N_C(t)$	The number of cancer cells at time t under homogeneous cancer model (HC model)
δ_0	The decay rate of cancer cells under the HC model
R_0	The replication rate of cancer cells under the HC model
μ	The probability that a hypertumor is produced due to the mutation during the replication of cancer cells under the HC model
ω_0	The net growth rate of cancer cells under HC model considering the decay and mutation defined as $\omega_0 \equiv (1-\mu)R_0 - \delta_0$
$H_C(t)$	The number of hypertumor cells at time t under the HC model
$R_{H,C}, R_{H,S}$	The replication rate of hypertumor cells under the HC model and CSC model, respectively
$\omega_{H,C}$	The net growth rate of hypertumor cells under HC model defined as $\omega_{H,C} \equiv R_{H,C} - \delta_0$
N^*	The number of cancer cells that results in the lethality of an organism
ρ_H^*	The ratio of hypertumor cells that arrests the cancer growth
t_C^*	The required time that the cancer size becomes N^*
z_C^*	The required time that the hypertumor ratio reaches ρ_H^* under the HC model, referred to as hypertumor saturation time (HST)
$\widetilde{z}_C^*$	Hypertumor saturation time when the effect of impeded in vivo tumor growth was considered (ivHST)
ψ	The probability that a cancer stem cell (CSC) divides symmetrically to produce two CSCs under the CSC model, given that no mutation occurs. With the probability of $1-\psi$, the asymmetric division produces one CSC and one bulk tumor cell (BTC) given that no mutation occurs. For simplicity, $\overline{\psi} = 1-\psi$
λ	The probability that a hypertumor is produced due to the mutation during the replication of CSCs. For simplicity, $\overline{\lambda} = 1-\lambda$
$N_S(t), N_P(t), H_S(t)$	The number of CSCs, BTCs, and hypertumors at time t, respectively, under CSC model.
R_S	The replication rate of CSCs
$\delta_S, \delta_P,$	The decay rates of CSCs and BTCs, respectively
t_S^*, z_S^*	Same as t_C^* and z_C^*, respectively, under the CSC model

Table 1. The description of the variables used in this study.

Meanwhile, if we set $\psi = 1$ [Eq. (12)] so that CSCs always produce CSCs (or hypertumor cells by mutation), then the CSC model is structurally identical to the HC model. This is intuitive as the HC model postulates all cancer cells, unless they are hypertumors, possess equipotent replication capability.

Evolutionary dynamics when state transition is allowed

As the most generalized model, a stochastic transition from one state to another can be postulated within the hierarchical framework. In the hierarchical model, there are two types of state transitions. The BTC may dedifferentiate into a CSC, and a strain of BTCs may transdifferentiate into another strain of BTCs. Let γ denote the rate of dedifferentiation that a BTC becomes a CSC.

Given that there is a single strain of BTCs,

$$\frac{dN_S(t)}{dt} = \left(\psi\overline{\lambda}R_S - \delta_S\right)N_S(t) + \gamma N_P(t), \tag{21}$$

$$\frac{dN_P(t)}{dt} = \overline{\psi}\,\overline{\lambda}R_S N_S(t) + (\omega_P - \gamma)N_P(t), \tag{22}$$

$$\frac{dH_S(t)}{dt} = (R_H - \delta_0)H(t) + \lambda R_S N_S(t). \tag{23}$$

The general solutions of $N_S(t)$ and $N_P(t)$ with arbitrary initial conditions are provided in Proposition 3.

In addition, suppose that there are m types of BTCs which exhibit identical dedifferentiation rates. Under these conditions, the sum of all types of BTCs should be identical to $N_P(t)$. Let $P_i(t)$ denote the size of the i-th BTC subpopulation. When a CSC produces a BTC, ε_i is the probability that a newly replicated BTC is of the i-th subpopulation. η_i is explained in Eq. (8), and $\alpha = \overline{\psi}\,\overline{\lambda}R_S$

In the form of a matrix differential equation,

$$\begin{bmatrix} N_S'(t) \\ P_1'(t) \\ P_2'(t) \\ \vdots \\ P_m'(t) \end{bmatrix} = \begin{bmatrix} \omega_S & \gamma & \gamma & \cdots & \gamma \\ \alpha\varepsilon_1 & \eta_1 & \tau_{2,1} & \cdots & \tau_{m,1} \\ \alpha\varepsilon_2 & \tau_{1,2} & \eta_2 & \cdots & \tau_{m,2} \\ \vdots & \vdots & \vdots & \ddots & \vdots \\ \alpha\varepsilon_m & \tau_{1,m} & \tau_{2,m} & \cdots & \eta_m \end{bmatrix} \begin{bmatrix} N_S(t) \\ P_1(t) \\ P_2(t) \\ \vdots \\ P_m(t) \end{bmatrix}. \tag{24}$$

Any BTC subpopulation which is produced by CSCs is persistent (Proposition 4). Although a BTC subpopulation is not produced by CSCs, if the relay of state transitions can lead to a transition from a persistent BTC subpopulation, such a BTC subpopulation is also persistent (Corollary 4).

Validation of the model to empirically observed data

Gupta et al.[10] measured the proportions of stem-like, basal, and luminal cancer lines from human breast cancer. To evaluate the validity of the model presented in this study, we fitted our model to changing proportions of the

actual cancer subpopulations among which state transition is possible. Let $S(t)$, $B(t)$, and $L(t)$ represent the number of the stem-like, basal, and luminal cancer lines at time t. Since the growth rate of each subpopulation is practically identical (denoted as w_0, refer to Fig. S1 of Gupta et al.[10]), the following matrix differential equation can be derived.

$$\dot{\mathbf{Z}}(t) = \begin{bmatrix} S'(t) \\ B'(t) \\ L'(t) \end{bmatrix} = \begin{bmatrix} w_0 - \tau_{1,2} - \tau_{1,3} & \tau_{2,1} & \tau_{3,1} \\ \tau_{1,2} & w_0 - \tau_{2,1} - \tau_{2,3} & \tau_{3,2} \\ \tau_{1,3} & \tau_{2,3} & w_0 - \tau_{3,1} - \tau_{3,2} \end{bmatrix} \begin{bmatrix} S(t) \\ B(t) \\ L(t) \end{bmatrix} = \mathbf{W}\mathbf{Z}(t). \quad (25)$$

As there were approximately 2.4 population doublings during 48 hours[10], it was postulated that $w_0 = 0.8318 \approx \ln\left[2^{2.4}\right]/2$ for SUM159 and SUM149 populations. Using manual digitization, we graphically extracted the observed composition of breast cancer lines (Fig. 3 of Gupta et al.[10]). The model with estimated coefficients is congruent to observed data (initial proportion, proportion at day 6, equilibrium proportion) (Fig. 2). The estimated coefficients used in the fitting for SUM159 populations are as follows.

$$\widehat{\mathbf{W}}_{\mathrm{SUM159}} = \begin{bmatrix} w_0 - 0.56 - 0.11 & 0.0154 & 0.0344 \\ 0.56 & w_0 - 0.0154 - 0.0013 & 0.7 \\ 0.11 & 0.0013 & w_0 - 0.0344 - 0.7 \end{bmatrix}. \quad (26)$$

Results of mathematical analyses (Proposition 2) imply that the finalized proportion itself cannot always uniquely determine the state transition rates, which could work as a guide or caveat for experimental researchers. For example, another set of estimated parameters results in similarly reliable fitting (dashed lines in Fig. 2a–c).

$$\widehat{\mathbf{W}}_{\mathrm{SUM159R}} = \begin{bmatrix} w_0 - 0.8398 - 0.11 & 0.0154 & 0.0344 \\ 0.8398 & w_0 - 0.0154 - 0.0013 & 0.4153 \\ 0.11 & 0.0013 & w_0 - 0.0344 - 0.4153 \end{bmatrix}. \quad (27)$$

In addition to SUM159 cancer populations, we applied our model to SUM149 population data which also results in reliable fitting results (Fig. 2d–f).

$$\widehat{\mathbf{W}}_{\mathrm{SUM149}} = \begin{bmatrix} w_0 - 0.12 - 0.43 & 0.02 & 0.005 \\ 0.12 & w_0 - 0.02 - 0.13 & 0.0006 \\ 0.43 & 0.13 & w_0 - 0.005 - 0.0006 \end{bmatrix}. \quad (28)$$

The estimated parameters imply that overall rates of state transition are lower than those of SUM159. This would be the reason that the observed proportion of SUM149 populations at day 6 is divergent from the equilibrium as shown in Gupta et al.[10]. It is predicted that it would take approximately 50 days for SUM149 populations to approach equilibrium (Fig. 2d–f).

Computational analysis

Implementation of long-term in vivo growth impediment

While the tumor growth of the early stage is well explained by exponential growth dynamics, a plethora of experimental results imply that tumor growth is impeded as the tumor size increases owing to hypoxia and limitations in nutrients[43–45] (Fig. 3a). For instance, if the active replication is restricted to the surface of the tumor cluster, the growth should follow a power function of time[43]. This prompted the development of intricate tumor growth models including the Mendelsohn model, Gompertz model, and von Bertalanffy model[43,44]. To implement the impeded yet positive growth of the tumor at the later stage of the progression, the time variable can be rescaled according to the following transformation (Fig. 3b).

$$f(t) = \tfrac{1}{\Psi}\ln\left[1 + \Psi t\right]. \quad (29)$$

The merit of such transformation is that it can demonstrate exponential tumor growth at an early stage and impeded growth governed by a power function at the later stage with minimal mathematical complexity (Fig. 3c,d).

Suppose that the time-scaling method is applied to $N_C(t)$ [Eq. (2)].

$$\widetilde{N}_C(t) = N_C(f(t)) = \exp\left[\tfrac{\omega_0}{\Psi}\ln\left[1 + \Psi t\right]\right] = (1 + \Psi t)^{\frac{\omega_0}{\Psi}}. \quad (30)$$

For $t \ll 1$,

$$\frac{d\widetilde{N}_C(t)}{dt} = \omega_0(1 + \Psi t)^{\frac{\omega_0}{\Psi} - 1} \approx \omega_0\left(1 + \omega_0 t - \Psi t\right) \approx \omega_0 \exp\left[\omega_0 t\right] = \frac{dN_C(t)}{dt} \quad (31)$$

which is intuitive to understand as $f(t) \approx t$ when t is sufficiently small.

For large t, we can approximate $\widetilde{N}_C(t)$ to power function $(\Psi t)^{\frac{\omega_0}{\Psi}}$ because

$$\lim_{t\to\infty} \frac{\widetilde{N}_C(t)}{(\Psi t)^{\frac{\omega_0}{\Psi}}} = 1. \quad (32)$$

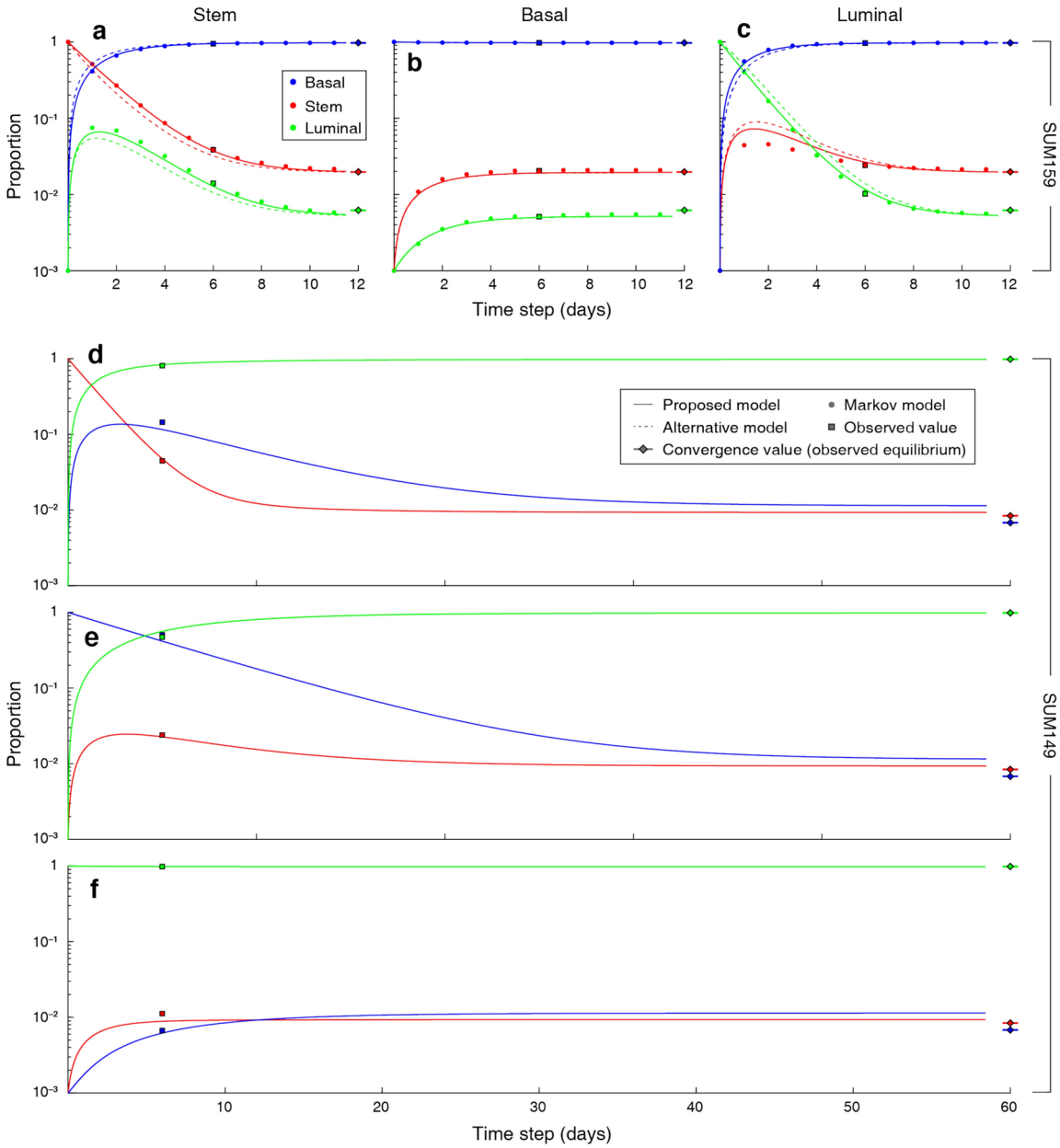

Fig. 2. The proposed model fitted to the observed data from Gupta et al.[10]. (**a**) The proportion changes of the SUM159 breast cancer lines when the initial population is composed of stem-like breast cancer cells. The proportions of basal, stem-like, and luminal cancer cells are illustrated with blue, red, and green markers or lines, respectively. The filled circles indicate the estimated proportions of the subpopulations based on the Markov process from Gupta et al.[10]. The rhombuses combined with short horizontal lines represent the asymptotic equilibrium obtained from the observed data. They are marked at day 12 in SUM159 lines and at day 60 in SUM149 lines. The solid lines are the fitted model based on equations proposed in this study [Eq. (26)]. The high fidelity of the alternative model [Eq. (27)] illustrated with dashed lines implies that state transition rates could be estimated in a different manner. For graphical simplicity, zero initial proportion was illustrated with 0.001. Explanations of the graphical elements are provided in the inset of (**d**) due to space limitations. (**b**) Same as (**a**) where the initial population is composed of basal breast cancer cells. In this panel, the solid and dashed lines are almost indistinguishable. (**c**) Same as (**a**) where the initial population is composed of luminal breast cancer cells. (**d**)–(**f**) We also fitted our model to the observed data of SUM149 populations [Eq. (28)]. Graphical components are identical to those in (**a**)–(**c**). As state-transition rates are generally lower than those of SUM159, it takes more time for SUM149 cells to reach the equilibrium.

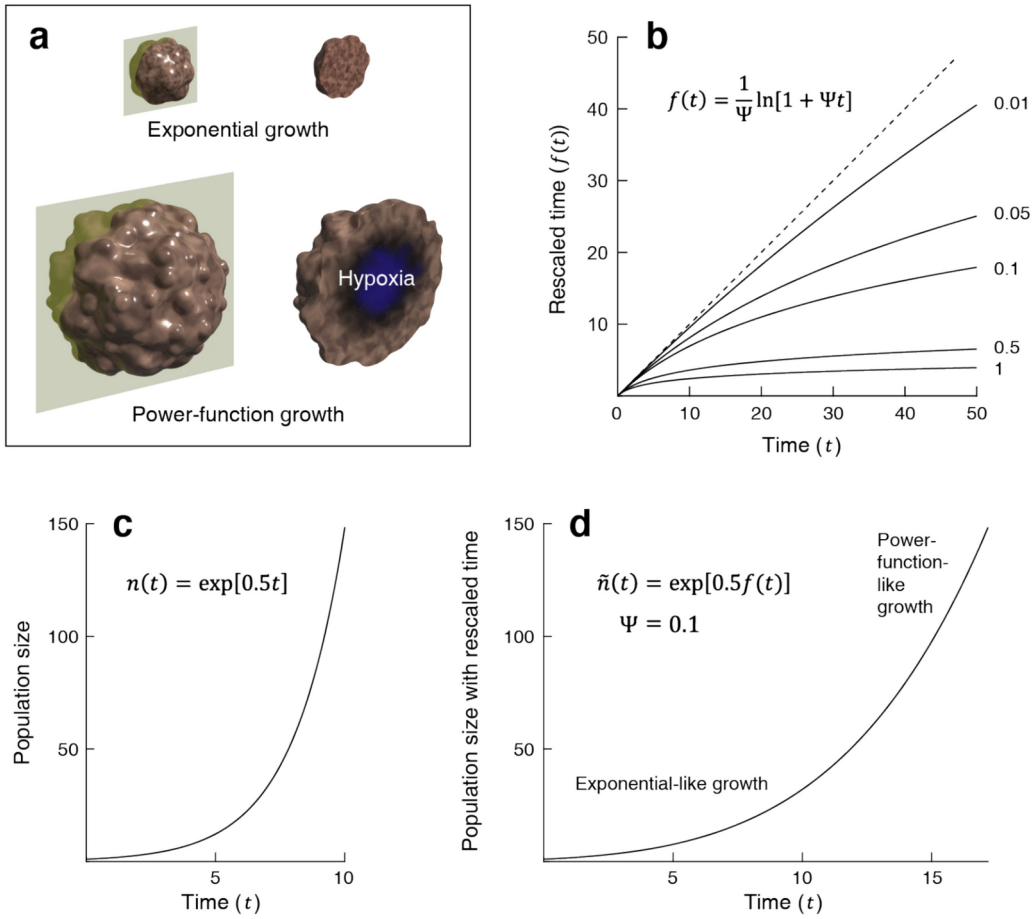

Fig. 3. The mathematical approach to implement impeded in vivo tumor growth at the later stage of tumor progression. (**a**) When in vivo tumor size is small, all tumor cells in the cluster would be oxygenated and nourished. If they replicate equally, the tumor grows exponentially. On the other hand, as tumor size becomes larger, the tumor cells in the central area of the cluster are inhibited from replicating. (**b**) To implement the attenuated growth at the later stage of the tumor progression, a specific transformation of time (time rescaling) was applied [Eq. (29)]. Specifically, by substituting t with $f(t)$ in equations postulating exponential growth, power-function-like growth at a later stage can be demonstrated. Here, Ψ represents the degree of growth suspension as higher Ψ results in the transition from exponential-like growth to power-function-like growth at the earlier phase of the tumor progression. The dashed line corresponds to the linear identity function ($f(t) = t$). (**c**) Suppose that the tumor size follows exponential growth of $n(t) = \exp[0.5t]$. (**d**) By substituting t with $f(t)$ in $n(t)$, we obtain $\widetilde{n}(t) = n(f(t)) = \exp[0.5f(t)]$. $\widetilde{n}(t)$ grows in an exponential-like manner when t is small, while it becomes power-function-like when t is large. This transformation allows us to capture the impeded tumor growth at a later stage.

Positive Ψ determines the degree of impeded in vivo growth: The higher Ψ is associated with the transition from exponential growth to power-function growth at the early phase of growth. Promoted angiogenesis will result in a lower value of Ψ in the model.

As such, when comparing simulation results of in vivo tumor growth under diverse parameters, we substituted the time terms of the generalized dynamics under HC and CSC models [Eqs. (2, 4, 15–17)] with the rescaled time.

$$\widetilde{N}_C(t) = N_C(f(t)), \widetilde{H}_C(t) = H_C(f(t)), \tag{33}$$

and

$$\widetilde{N}_S(t) = N_S(f(t)), \widetilde{N}_P(t) = N_P(f(t)), \widetilde{H}_S(t) = H_S(f(t)). \tag{34}$$

Likewise, we can define in vivo HST (ivHST) under the HC model ($\widetilde{z}_C^*$) such that

$$\frac{\widetilde{H}_C\left(\widetilde{z}_C^*\right)}{\widetilde{N}_C\left(\widetilde{z}_C^*\right)} = \rho_H^* \tag{35}$$

where $\widetilde{z}_C^* = f^{-1}(z_C^*)$. Similarly, ivHST under the CSC model can be defined as $\widetilde{z}_S^* = f^{-1}(z_S^*)$.

Note that $f : [0, \infty] \to [0, \infty]$ is a monotonic bijective function, hence $t_1 < t_2$ implies that $f(t_1) < f(t_2)$. In addition, a change in time scale does not affect the eventual cancer size (at ivHST) because $N_C(\widetilde{z}_C^*) = N_C(f(\widetilde{z}_C^*)) = N_C(z_C^*) = U_C^*$.

Comparison of growth dynamics

Cancer progression under HC and CSC models was analyzed by computationally solving differential equations for cancer and hypertumor growth, incorporating in vivo growth impediments. If the replication fidelity of the CSCs is sufficiently lower than that of the homogeneous cancer cells ($\mu = 0.02, \lambda = 0.001$), the eventual cancer size (the tumor cluster size at ivHST) is larger under the CSC model than that of the HC model ($U_S^* > U_C^*$ in Fig. 4a,b). However, until the ivHST of the HC model ($\widetilde{z}_C^*$), the cancer cluster size under the HC model is larger than the size under the CSC model (Fig. 4b). If the cancer cluster that induces lethality is small enough (N_1^* in Fig. 4b), then homogeneous cancer cells will reach that lethal size faster than hierarchical cancer cells ($\widetilde{t}_{C,1}^* < \widetilde{t}_{S,1}^*$). On the other hand, if the lethal cancer size is greater than the eventual cancer size under the HC model yet smaller than the eventual cancer size under the CSC model ($U_C^* < N_2^* < U_S^*$ in Fig. 4b), only hierarchical cancer cells can exhibit lethality.

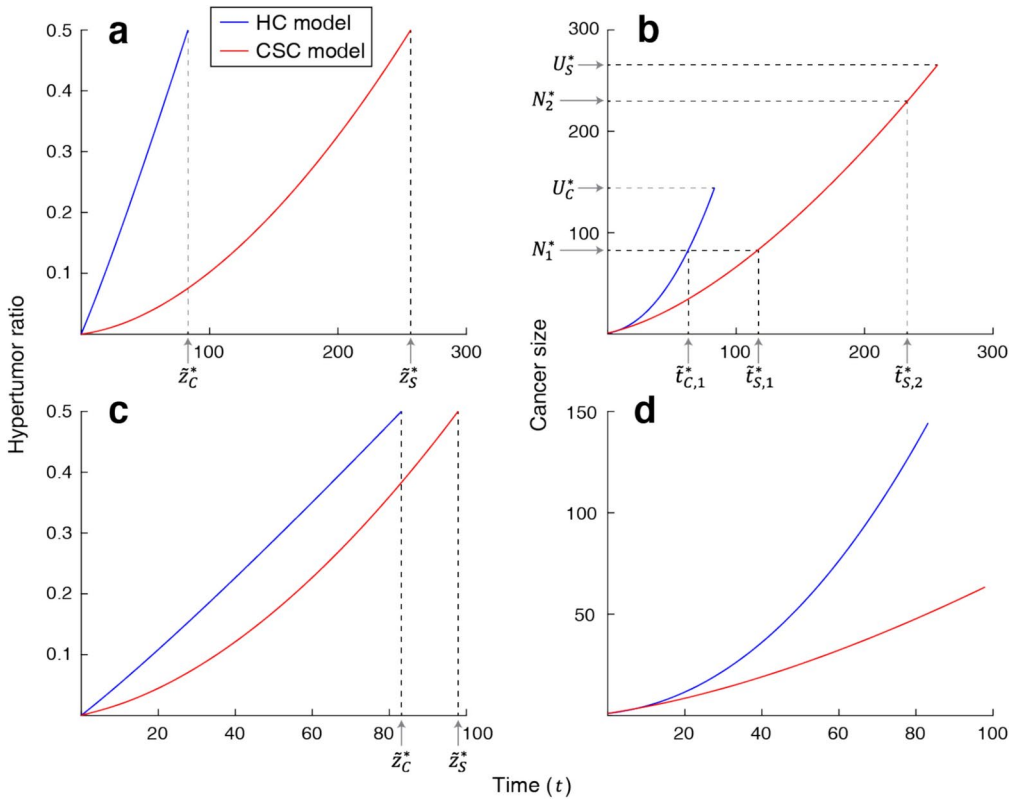

Fig. 4. The computational results of hypertumor and cancer growth under the homogeneous cancer model (HC model) and cancer stem cell model (CSC model). (**a**) We posited that the cancer cluster cannot expand anymore if the ratio of hypertumor cells to cancer cells reaches 0.5 ($\rho_H^* = 0.5$ in Eqs. (6) and (20)). The model parameters are: $\psi = 0.5$, $R_S = 1/3$, $\delta_S = 0.01$, $\delta_P = 1/7$, $R_0 = 1/4$, $\delta_0 = 1/45$, $R_{H,S} = R_{H,C} = 1/2.8$, $\mu = 0.02$, $\lambda = 0.001$ on assumption that the replication fidelity of cancer stem cells is higher than homogeneous cancer cells (i.e., $\mu > \lambda$). The blue and the red line represent the hypertumor ratio under the HC model and CSC model, respectively. Note that time rescaling was applied to implement the impeded tumor growth at the later stage [Eq. (29)]. Hypertumor ratio reaches ρ_H^* at $\widetilde{z}_C^*$ and $\widetilde{z}_S^*$ under HC model and CSC model, respectively (in vivo hypertumor saturation time, ivHST). (**b**) The dynamics of the cancer size under the HC model (blue line) and CSC model (red line). Suppose that the cluster becomes lethal when it reaches the size of N_1^*. As shown in the graph, the time it takes for a cancer cluster to reach N_1^* is shorter for the homogeneous cluster compared to the hierarchical cluster ($\widetilde{t}_{C,1}^* < \widetilde{t}_{S,1}^*$). In contrast, cancer cluster under the HC model cannot reach the size of N_2^* because the hypertumor ratio becomes 0.5 before then. Only cancer clusters under the CSC model can attain the size of N_2^*. U_C^* and U_S^* are the eventual cancer size (the cancer size at ivHST) of the HC model and CSC model, respectively. (**c**) Same as (**a**) except that $\lambda = 0.005$. The hypertumor ratio under the HC model reaches ρ_H^* within a shorter time compared to the CSC model. (**d**) Same as (**b**) except that $\lambda = 0.005$. In this condition, though there is more time for the cancer cluster under the CSC model to expand, the cancer cluster under the HC model grows faster.

If the replication fidelity of CSCs is not sufficiently higher than that of the homogeneous cells ($\mu = 0.02$, $\lambda = 0.005$), the eventual cancer size under the HC model could be larger than that under the CSC model (Fig. 4d). Moreover, homogeneous cancer cells grow faster than hierarchical cancerous cells. In both conditions, the ivHST of the HC model is shorter than that of the CSC model ($\widetilde{z}_C^* < \widetilde{z}_S^*$ in Fig. 4a,c).

In order to comprehensively compare the growth of the cancer clusters in the presence and the absence of the hierarchy, cancer progression dynamics were computationally solved under a range of parameters. Similar to the high fidelity of normal stem cells[46], CSCs are more resilient to mutations compared to BTCs by reducing reactive oxygen species[47,48]. Based on this trait, we posited that the replication fidelity of CSCs is higher than homogeneous cancer cells of the same replication rate. As the number of cell replications is a reliable estimator of the accumulated mutation[49], a higher replication rate of the CSCs was assumed to elevate the emergence of the hypertumors. In this model, the probability of hypertumor emergence during the replication of the CSCs is proportional to the replication rate. The specific relation between CSC replication rate and hypertumor generation is provided in Supplementary Materials (Eq. [S68]).

For fixed parameters for the HC model, the parameters of the CSC replication rate (R_S) and self-renewal probability (ψ) were varied. We adopted the HSB (HSV) color system to compare the cancer progression dynamics of the two systems. We identified the vector whose horizontal component is the difference of ivHST ($\widetilde{z}_S^* - \widetilde{z}_C^*$) and the vertical component is the difference in eventual cancer size multiplied by a scalar factor ($s\,(U_S^* - U_C^*)$) where $s = 0.05$. Let this vector be denoted as the comparison vector. If the cancer reaches maximal lethal size (cancer size of 10^{10}) before the hypertumor reaches the arrest ratio (ρ_H^*), ivHST was set to be the time at which the maximal lethal size is reached. In this case, the eventual cancer size is identical to the maximal lethal size.

The direction of the comparison vector is illustrated with hue (0° to 360°). The saturation of the color is determined by the length of this vector with a specific transformation. Hence, achromatic color (low saturation) implies that the vector is short. For a model that can reach a larger eventual cancer size, the range of the cancer size in which that model takes a shorter time to attain that size was reflected in the brightness (value) of the color. For example, although the HC model can gain a larger eventual cancer size ($U_S^* < U_C^*$) in Fig. 5a, cancer cells under the CSC model can reach small cancer size in a shorter time (red vertical bar). In this case, the color becomes less bright. The computational results are presented in Fig. 5b–g.

Discussion

In lieu of the conventional understanding that a tumor is composed of homogeneous mutated cells, it became widely accepted that there is a hierarchical structure in cancer more prevalent than previously appreciated[1,4]. Due to this hierarchy, the elimination of BTCs may give a misguided conclusion that the cancer has regressed though the paucity of remaining CSCs are intact. Hence, the therapeutic sensitivity and relapse potential of CSCs are of particular interest to biomedical researchers[1].

In the meantime, the possible presence and implications of the defective hypertumors have been proposed[22]. Along with higher evolutionary pressure of the cancer suppression in larger and longer-living animals[30] supported by the elaborate anticancer mechanisms in those animals[36,50], the spontaneous generation of the hypertumor within the cancer cluster was suggested as the grounds of Peto's paradox[23]. Given that cells with identical mutations cooperate via diffusive cancer growth factors, they may satisfy the conditions of the green-beard effect[20]. Within this framework, hypertumor is the false beard[19,20], whose fitness is reliant on the recognition error of cooperators[51] mediated by the nondiscriminatory cancer growth factors. By employing the cooperative characteristics of the cancer cells, implementation of the defectors would jeopardize the integrity of the cancer cluster, conceptualized as autologous cell defection[25].

Stem cells, normal or cancerous, occupy the pinnacle of the hierarchy whose fidelity determines the overall stability of the progeny cells[52]. This imposes higher evolutionary pressure for stem cells or CSCs to sustain higher replication fidelity as evidenced by empirical findings[46–48].

Cancer is not an exception in small multicellular animals including *Hydra*, Planarians, and *Drosophila*[53]. For larger animals (e.g., whales or elephants), N^* should be much larger than that of smaller animals[23]. As shown in Eqs. (5) and (19), larger N^* increases the time it takes to reach detrimental cancer size under the CSC model and HC model. It would be difficult for the cancer cluster to reach the detrimental size if hypertumors predominate rapidly. In a mathematical sense, this implies $t_C^* > z_C^*$ (equivalently, $\widetilde{t}_C^* > \widetilde{z}_C^*$) for HC model and $t_S^* > z_S^*$ (equivalently, $\widetilde{t}_S^* > \widetilde{z}_S^*$) for the CSC model. It should be noted that t_C^* and t_S^* (together with $\widetilde{t}_C^*$ and $\widetilde{t}_S^*$) increase as N^* increases, while z_C^* and z_S^* (as well as $\widetilde{z}_C^*$ and $\widetilde{z}_S^*$) are independent to N^*. Therefore, for a sufficiently large N^*, we can expect that $\widetilde{z}_C^*$ and $\widetilde{z}_S^*$ will become the limiting factor for a cancer cluster to reach N^* (Fig. 6).

In support of this argument, our comprehensive computational results demonstrate there are specific sets of conditions including the existence of hierarchy, CSC replication rate, and CSC self-renewal rate that are favorable to reaching the lethal cancer size in a shorter period of time. Based on the results shown in Fig. 5, cancers that lead to the lethality of large animals might be hierarchical and equipped with a high self-renewal rate while those for small animals might be relatively homogeneous. This implies that the cancer hierarchy of small and large animals may be different. With advanced single-cell analysis techniques[54], subsequent investigations of necropsy (or autopsy)[36] samples will be required to validate this argument.

As previously reported, different types of cancers exhibit different hierarchies. Furthermore, the hierarchy is not organ-specific: Though not conclusive, the hierarchy may be present or absent in the same type of tumor[2]. Underpinned by differences in mutations responsible for leukemic identical twins[55], it appears that stochasticity plays a central role in cancer progression, diversifying possible outcomes of the cancer structure. Considering these findings, cancers with different hierarchical structures may arise within the same organism, influencing the probability of lethality.

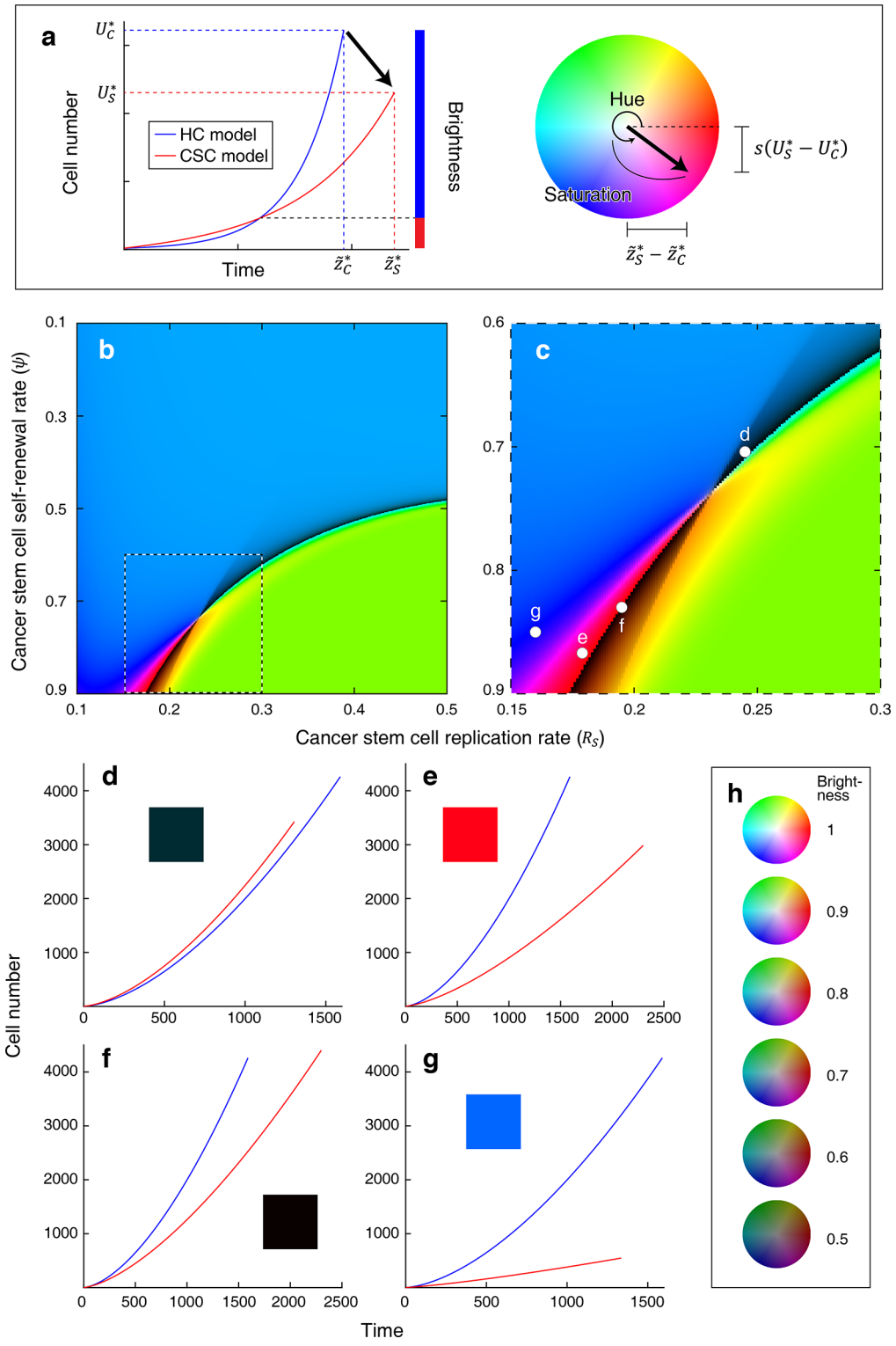

Employing the hypertumor model focusing on blood vessel formation, Nagy[23] computationally investigated the cancer susceptibility across animals of different body mass and lifespan. As larger animals require a proportionally larger tumor to reach lethality, the time required for a lethal tumor to develop and cause mortality is correspondingly prolonged in larger animals, during which hypertumor is likely to appear. Hence, Nagy[23] showed that emergent hypertumor leads to tumor suppression in large animals. In other words, the absence of hypertumor development should be the prerequisite for the tumor to become lethal for larger animals in Nagy's[23] study. This is in the same line with our model in that hypertumor acts as a constraint for the maximal tumor size. Our study adds a new layer of understanding with respect to the hierarchical structures of the lethal tumors across species. Given that cancer stem cells have higher fidelity of replication, we propose that lethal tumors of large animals would be composed of cancer stem cells and bulk tumor cells. In contrast, homogeneous

◀**Fig. 5**. Comparison of HC and CSC model under diverse parameters. (**a**) To illustrate the discrepancy between the two cancer progression models, we devised a comparison vector (black arrow) whose horizontal component is $\widetilde{z}_S^* - \widetilde{z}_C^*$ and the vertical component is $s(U_S^* - U_C^*)$. Here, s is the scale factor ($s = 0.05$). The positive angle of the comparison vector from the x-axis corresponds to the hue and the length of the vector is positively associated with the saturation of the color. For example, a comparison vector whose angle is 0° is marked in red. The range of cancer size that requires less time for the models to reach that size determines the brightness. In this example, brightness is less than 1 as cancer under the CSC model can reach the small cancer size in a shorter time (red vertical bar), although cancer under the HC model has a higher eventual cancer size. (**b**) For fixed parameters of the HC model, we varied the parameters of cancer stem cell replication rate (R_S) and self-renewal rate (ψ). At each grid on the plane, the cancer progression of the two models was represented with HSB color schematics explained in (**a**). The eventual cancer size of the CSC model is larger in the light green region. Higher replication rates of cancer stem cells accordingly elevate the hypertumor-inducing mutations (Eq. [S68]). The region delineated by an alternating white-and-black dashed line is shown in (**c**). (**c**) Magnified image of the delineated region in (**b**). Cancer progression in four points is illustrated in (**d**)–(**g**). (**d**) The in vivo hypertumor saturation time of the HC model is 1589.9 with an eventual cancer size of 4260. For $R_S = 0.245$ and $\psi = 0.704$, the eventual cancer size under the CSC model is smaller. Note that the dynamics of cancer progression under the HC model are identical in (**d**)–(**g**). The inset color represents the grid color in (**c**). (**e**) Same as (**d**) for $R_S = 0.179$ and $\psi = 0.867$. (**f**) Same as (**d**) for $R_S = 0.195$ and $\psi = 0.83$. (**g**) Same as (**d**) for $R_S = 0.16$ and $\psi = 0.85$. (**h**) The HSB color schematics with brightness from 0.5 to 1.

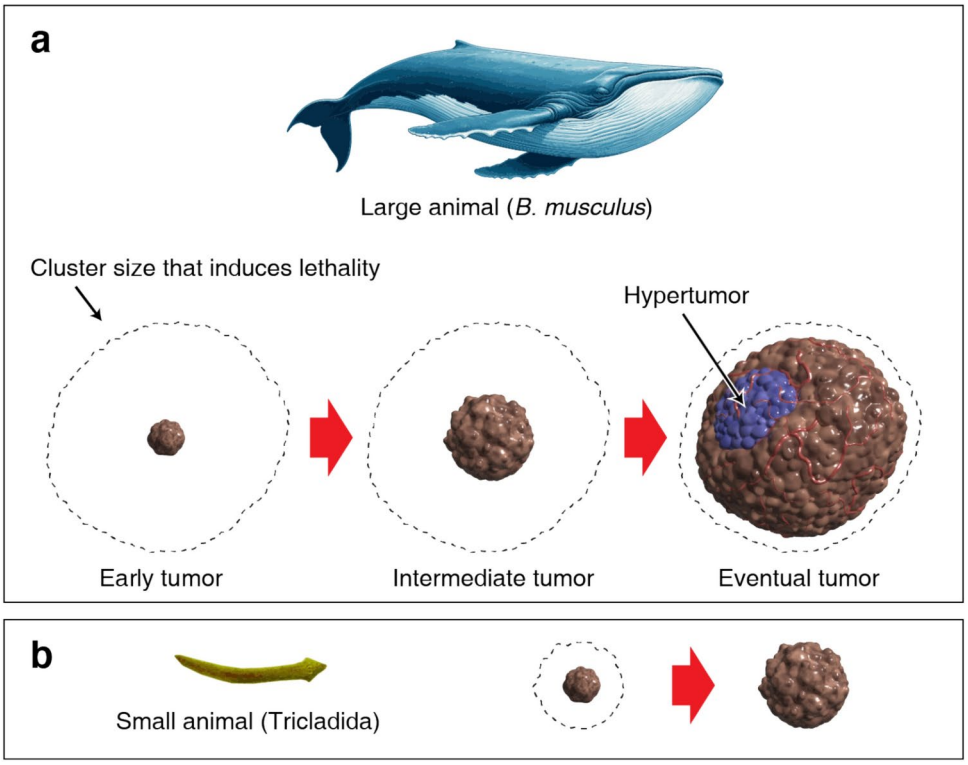

Fig. 6. The possible trade-off of the homogeneous and hierarchical cancer cluster. (**a**) For a larger animal, the tumor should be proportionally larger to become lethal (dashed outlines). As it takes a longer time for a tumor to reach a larger size, a group of hypertumors (blue cluster) may appear which will hinder that cancer cluster from reaching the lethal size. Hence, only hierarchical cancer clusters containing cancer stem cells with higher replication fidelity might become lethal in large animals. The effect of the hypertumor on a large cancer cluster was suggested as a principle to explain Peto's paradox. (**b**) For a small animal, the tumor size that becomes lethal would be correspondingly small. The time for a cancer cluster to reach the lethal size is accordingly small. As a hypertumor is unlikely to appear and propagate within such a short time, homogeneous cancer cells—each endowed with replication capability—might reach a lethal size faster than hierarchical cancer clusters.

tumor cells despite their enhanced susceptibility to hypertumors could promptly reach the size of the lethality for small animals.

Mutated cells responsible for leukemias and tumors exhibit different degrees of mobility[56,57]. Additionally, it was revealed by biopsy data that subpopulations of tumors could be spatially clustered or blended[13,15,58].

Therefore, hypertumor cells in a spatially relaxed environment would be blended with other cancer cells, while hypertumor cells with little mobility are likely to be clustered[59]. A previous simulation study that reflected cancer growth factor diffusion indicated that the spatial structure of cancer cells and hypertumor cells has a significant impact on hypertumor progression[26]. For example, hypertumor cells adjacent to hypertumor–cancer interface are expected to gain substantial fitness while those at the central region of the large hypertumor cluster would have lower fitness as they are deprived of growth factors produced by cancer cells[26]. In contrast, cancer cells at the periphery of the cancer cluster will have lower fitness compared to those in the central part of the cancer cluster, again due to the difference in cancer growth factor exposure[26]. Hence, the fitness of cancer and hypertumor cells is not constant as postulated in this study but dependent on their spatial configuration which will fluctuate as the tumor progresses. Furthermore, the hierarchy established by cancer stem cells could be more complicated than previously perceived[1]. Subsequent studies should embrace the effect of spatial structure, competition among diverse subpopulations, and sophisticated hierarchy.

In conclusion, this is the first study, to our knowledge, that bridges the gap between cancer hierarchy and hypertumor progression. Pioneering experiments designed to verify autologous cell defection should consider such a cancer hierarchy. For instance, free radical scavengers of CSCs could be suppressed[48] to elevate the mutation rate and to promote the development of hypertumors. The site-directed mutagenesis in genes responsible for the cancer growth factors or tumor microenvironment establishment at CSCs could promote spontaneous hypertumor formation. The framework established in this study will lay conceptual foundations for novel anticancer strategies.

Data availability

The MATLAB code used to derive the computational results is available at https://zenodo.org/records/15033596.

Received: 25 June 2024; Accepted: 14 March 2025
Published online: 03 April 2025

References

1. Batlle, E. & Clevers, H. Cancer stem cells revisited. *Nat. Med.* **23**, 1124–1134 (2017).
2. Shackleton, M., Quintana, E., Fearon, E. R. & Morrison, S. J. Heterogeneity in cancer: Cancer stem cells versus clonal evolution. *Cell* **138**, 822–829 (2009).
3. Kreso, A. & Dick, J. E. Evolution of the cancer stem cell model. *Cell Stem Cell* **14**, 275–291 (2014).
4. Rich, J. N. Cancer stem cells: understanding tumor hierarchy and heterogeneity. *Medicine* **95**, S2–S7 (2016).
5. Ghiaur, G., Gerber, J. & Jones, R. J. Concise review: Cancer stem cells and minimal residual disease. *Stem Cells* **30**, 89–93 (2012).
6. Quintana, E. et al. Efficient tumour formation by single human melanoma cells. *Nature* **456**, 593–598 (2008).
7. Vermeulen, L. et al. Wnt activity defines colon cancer stem cells and is regulated by the microenvironment. *Nat. Cell Biol.* **12**, 468–476 (2010).
8. Quintana, E. et al. Phenotypic heterogeneity among tumorigenic melanoma cells from patients that is reversible and not hierarchically organized. *Cancer Cell* **18**, 510–523 (2010).
9. Williams, R. T., Den Besten, W. & Sherr, C. J. Cytokine-dependent imatinib resistance in mouse BCR-ABL+ Arf-null Lymphoblastic leukemia. *Genes Dev.* **21**, 2283–2287 (2007).
10. Gupta, P. B. et al. Stochastic state transitions give rise to phenotypic equilibrium in populations of cancer cells. *Cell* **146**, 633–644 (2011).
11. Ågren, J. A. *The Gene's-Eye View of Evolution* (Oxford University Press, 2021).
12. Burrell, R. A., McGranahan, N., Bartek, J. & Swanton, C. The causes and consequences of genetic heterogeneity in cancer evolution. *Nature* **501**, 338–345 (2013).
13. Gerlinger, M. et al. Intratumor heterogeneity and branched evolution revealed by multiregion sequencing. *New England J. Med.* **366**, 883–892 (2012).
14. Anderson, K. et al. Genetic variegation of clonal architecture and propagating cells in leukaemia. *Nature* **469**, 356–361 (2011).
15. Yachida, S. et al. Distant metastasis occurs late during the genetic evolution of pancreatic cancer. *Nature* **467**, 1114–1117 (2010).
16. Kreso, A. et al. Variable clonal repopulation dynamics influence chemotherapy response in colorectal cancer. *Science* **339**(6119), 543–548 (2013).
17. Notta, F. et al. Evolution of human BCR–ABL1 lymphoblastic leukaemia-initiating cells. *Nature* **469**, 362–367 (2011).
18. Wang, W. et al. Dynamics between cancer cell subpopulations reveals a model coordinating with both hierarchical and stochastic concepts. *PLoS One* **9**(1), e84654 (2014).
19. Archetti, M. & Pienta, K. J. Cooperation among cancer cells: Applying game theory to cancer. *Nat. Rev. Cancer* **19**, 110–117 (2019).
20. Capp, J. P. et al. The paradox of cooperation among selfish cancer cells. *Evol. Appl.* **16**, 1239–1256 (2023).
21. Archetti, M. Dynamics of growth factor production in monolayers of cancer cells and evolution of resistance to anticancer therapies. *Evol. Appl.* **6**, 1146–1159 (2013).
22. Nagy, J. D. Competition and natural selection in a mathematical model of cancer. *Bull Math. Biol.* **66**, 663–687 (2004).
23. Nagy, J. D., Victor, E. M. & Cropper, J. H. Why don't all whales have cancer? A novel hypothesis resolving Peto's paradox. *Integr. Comp. Biol.* **47**, 317–328 (2007).
24. Archetti, M. Collapse of intra-tumor cooperation induced by engineered defector cells. *Cancers (Basel)* **13**(15), 3674 (2021).
25. Archetti, M. Evolutionarily stable anti-cancer therapies by autologous cell defection. *Evol. Med. Public Health* **2013**, 161–172 (2013).
26. Choi, J. Spatial simulation of autologous cell defection for cancer treatment. *Evol. Med. Public Health* **11**, 461–471 (2023).
27. Peto, H., Roe, F. J. C., Lee, P. N., Levy, L. & Clack, J. Cancer and ageing in mice and men. *Br. J. Cancer* **32**, 411–426 (1975).
28. Caulin, A. F. & Maley, C. C. Peto's Paradox: Evolution's prescription for cancer prevention. *Trends Ecol. Evol.* **26**, 175–182 (2011).
29. Nunney, L. The real war on cancer: The evolutionary dynamics of cancer suppression. *Evol. Appl.* **6**, 11–19 (2013).
30. Brown, J. S., Cunningham, J. J. & Gatenby, R. The multiple facets of peto's paradox: A life-history model for the evolution of cancer suppression. *Philosoph. Trans. Royal Soci. B: Biol. Sci.* **370**(1673), 20140221 (2015).
31. Roche, B., Sprouffske, K., Hbid, H., Missé, D. & Thomas, F. Peto's paradox revisited: Theoretical evolutionary dynamics of cancer in wild populations. *Evol. Appl.* **6**, 109–116 (2013).
32. Nunney, L. Resolving Peto's paradox: Modeling the potential effects of size-related metabolic changes, and of the evolution of immune policing and cancer suppression. *Evol. Appl.* **13**, 1581–1592 (2020).
33. Stiehl, T. & Marciniak-Czochra, A. Mathematical modeling of leukemogenesis and cancer stem cell dynamics. *Math. Model Nat. Phenom.* **7**, 166–202 (2012).

34. Michor, F. Mathematical models of cancer stem cells. *J. Clin. Oncol.* **26**, 2854–2861 (2008).
35. Vainstein, V., Kirnasovsky, O. U., Kogan, Y. & Agur, Z. Strategies for cancer stem cell elimination: Insights from mathematical modeling. *J. Theor. Biol.* **298**, 32–41 (2012).
36. Abegglen, L. M. et al. Potential mechanisms for cancer resistance in elephants and comparative cellular response to DNA Damage in Humans. *JAMA – J. Am. Med. Associat.* **314**, 1850–1860 (2015).
37. Murray, D. L. & Sandercock, B. K. *Population Ecology in Practice* (Wiley, 2020).
38. Rodriguez-Brenes, I. A., Komarova, N. L. & Wodarz, D. Tumor growth dynamics: Insights into evolutionary processes. *Trends Ecol. Evol.* **28**, 597–604 (2013).
39. Driessens, G., Beck, B., Caauwe, A., Simons, B. D. & Blanpain, C. Defining the mode of tumour growth by clonal analysis. *Nature* **488**, 527–530 (2012).
40. Pardal, R., Clarke, M. F. & Morrison, S. J. Applying the principles of stem-cell biology to cancer. *Nat. Rev. Cancer* **3**, 895–902 (2003).
41. Hayflick, L. The limited in vitro lifetime of human diploid cell strains. *Exp. Cell Res.* **37**, 614–636 (1965).
42. Hayflick, L. & Moorhead, P. S. The serial cultivation of human diploid cell strains. *Exp. Cell Res.* **25**, 585–621 (1961).
43. Gerlee, P. The model muddle: In search of tumor growth laws. *Cancer Res.* **73**, 2407–2411 (2013).
44. Sarapata, E. A. & De Pillis, L. G. A comparison and catalog of intrinsic tumor growth models. *Bull Math Biol* **76**, 2010–2024 (2014).
45. Brú, A., Albertos, S., Subiza, J. L., García-Asenjo, J. L. & Brú, I. The universal dynamics of tumor growth. *Biophys J* **85**, 2948–2961 (2003).
46. Cervantes, R. B., Stringer, J. R., Shao, C., Tischfield, J. A. & Stambrook, P. J. Embryonic stem cells and somatic cells differ in mutation frequency and type. *Proceed. Nat. Acad. Sci.* **99**, 3586–3590 (2002).
47. Bao, S. et al. Glioma stem cells promote radioresistance by preferential activation of the DNA damage response. *Nature* **444**, 756–760 (2006).
48. Diehn, M. et al. Association of reactive oxygen species levels and radioresistance in cancer stem cells. *Nature* **458**, 780–783 (2009).
49. Uchinomiya, K. & Tomita, M. A mathematical model for cancer risk and accumulation of mutations caused by replication errors and external factors. *PLoS One* https://doi.org/10.1371/journal.pone.0286499 (2023).
50. Gorbunova, V., Seluanov, A., Zhang, Z., Gladyshev, V. N. & Vijg, J. Comparative genetics of longevity and cancer: Insights from long-lived rodents. *Nat. Rev. Genet.* **15**, 531–540 (2014).
51. Choi, J., Lee, S., Kim, H. & Park, J. The role of recognition error in the stability of green-beard genes. *Evol. Lett.* **7**, 157–167 (2023).
52. Tomasetti, C. & Vogelstein, B. Variation in cancer risk among tissues can be explained by the number of stem cell divisions. *Science* **347**(6217), 78–81 (2015).
53. Aktipis, A. C. et al. Cancer across the tree of life: Cooperation and cheating in multicellularity. *Philosoph. Trans. Royal Soci. B: Biol. Sci.* https://doi.org/10.1098/rstb.2014.0219 (2015).
54. Smith, E. A. & Hodges, H. C. The spatial and genomic hierarchy of tumor ecosystems revealed by single-cell technologies. *Trends Cancer* **5**, 411–425 (2019).
55. Bateman, C. M. et al. Acquisition of genome-wide copy number alterations in monozygotic twins with acute lymphoblastic leukemia. *Blood* **115**, 3553–3558 (2010).
56. Asada, N. et al. Matrix-embedded osteocytes regulate mobilization of hematopoietic stem/progenitor cells. *Cell Stem Cell* **12**, 737–747 (2013).
57. Pathak, A., Kumar, S. & Discher, D. E. Independent regulation of tumor cell migration by matrix stiffness and confinement. *Proceed. Nat. Acad. Sci.* **109**, 10334–10339 (2012).
58. Wu, H. J. et al. Spatial intra-tumor heterogeneity is associated with survival of lung adenocarcinoma patients. *Cell Genomics* https://doi.org/10.1016/j.xgen.2022.100165 (2022).
59. Bi, D., Yang, X., Marchetti, M. C. & Manning, M. L. Motility-driven glass and jamming transitions in biological tissues. *Phys. Rev. X* **6**, 021011 (2016).

Acknowledgements

J. C. was supported by the National Research Foundation of Korea (NRF) grant funded by the Korea government (MSIT) (No. 2021R1A6A3A01086754, No. RS-2024-00337511). S. L. was supported by the National Research Foundation of Korea (NRF) grant funded by the Korean government (MSIT) (No. 2022R1A5A1033624). J. P. and S. K. were supported by the National Research Foundation of Korea (NRF) grant funded by the Korea government (MSIT) (No. NRF-2023R1A2C1004893).

Author contributions

J. C. conceptualized this study and wrote the original draft. J. C., S. K., S. L., J. P. conducted the mathematical and computational analysis. J. C. and J. P. reviewed and revised the manuscript.

Declarations

Competing interests

The authors have no conflicts of interest to declare.

Additional information

Supplementary Information The online version contains supplementary material available at https://doi.org/10.1038/s41598-025-94852-y.

Correspondence and requests for materials should be addressed to J.C. or J.P.